UCLA
UCLA Previously Published Works

## Title

Interpreting the Operando XANES of Surface-Supported Subnanometer Clusters: When Fluxionality, Oxidation State, and Size Effect Fight

## Permalink

https://escholarship.org/uc/item/3pg4255s

## Journal

The Journal of Physical Chemistry C, 124(18)

## ISSN

1932-7447

## Authors

Zandkarimi, Borna
Sun, Geng
Halder, Avik
et al.

## Publication Date

2020-05-07

## DOI

10.1021/acs.jpcc.0c02823

Peer reviewed

eScholarship.org Powered by the California Digital Library
University of California

# Interpreting *operando* XANES of Surface-supported Subnanometer Clusters: When Fluxionality, Oxidation State and Size Effect Fight

*Borna Zandkarimi,[a] Geng Sun,[b] Avik Halder,[c] Soenke Seifert,[d] Stefan Vajda,[c,e,f] Philippe Sautet,[a,b,g*] and Anastassia N. Alexandrova[a,g*]*

[a]Department of Chemistry and Biochemistry, University of California, Los Angeles, Los Angeles, CA 90095

[b]Department of Chemical and Biomolecular Engineering, University of California, Los Angeles, Los Angeles, California 90095, United States

[c]Materials Science Division, Argonne National Laboratory, Argonne Illinois 60439, United States

[d]X-ray Science Division, Argonne National Laboratory, 9700 South Cass Avenue, Argonne, Illinois 60439, United States

[e]Institute for Molecular Engineering, The University of Chicago, 5640 South Ellis Avenue, Chicago, Illinois 60637, USA

[f]Department of Nanocatalysis, J. Heyrovský Institute of Physical Chemistry, Czech Academy of Sciences, Dolejškova 3, 18223Prague 8, Czech Republic

[g]CaliforniaNanoSystems Institute, 570 Westwood Plaza, Los Angeles, CA 90095

*Corresponding Authors: Philippe Sautet, (310) 825-8485, sautet@ucla.edu, Anastassia N. Alexandrova, (310) 825-3769, ana@chem.ucla.edu

## Abstract

X-ray absorption near edge structure (XANES) spectroscopy is widely used for *operando* catalyst characterization. We show that, for highly fluxional supported nanoclusters, the customary extraction of the oxidation state of the metal from the XANES data by fitting to the bulk standards is highly questionable. The XANES signatures, as well as the apparent oxidation state for such clusters arise from a complex combination of many factors, and not only from the chemical composition in reaction conditions (e.g. oxygen content in oxidizing astrosphere). The thermally-accessible isomerization and population of several structurally distinct cluster forms, cluster-support interaction, and intrinsic size effects all impact the metal oxidation state and XANES signal. We demonstrate this on copper oxide clusters with different compositions, $Cu_4O_x$(x = 2–5) and $Cu_5O_y$ (y = 3, 5), deposited on amorphous alumina and ultrananocrystalline diamond (UNCD), for which we computed the XANES spectra and compare the results to the experiment. We show in addition that fitting the experimental spectrum to calculated spectra of supported clusters can in contrast provide good agreement and insight on the spectrum-composition-structure relation. Experimental XANES interpreted using the proposed fitting scheme shows the partial reduction of Cu oxide clusters at rising temperatures, and pinpoints the specific stoichiometries that dominate in the ensemble of cluster states as the temperature changes.

## Introduction

Over the past few decades, there have been considerable advances in understanding the X-ray absorption near edge structure (XANES).[1–3] The strong scattering of the photoelectron and weak inelastic losses in this region, which is within ca. 30 eV of threshold, make XANES a powerful technique to reveal the structure of systems of interest.[2] XANES has been used to extract relevant information such as oxidation state and geometry of inorganic metal complexes as well as metal and metal oxide surfaces.[4–8] XANES is sensitive to geometry and to the oxidation state of the metal center, which makes it an important tool to distinguish between different structures.[9–12] The pre-edge region can be used to estimate the ligand field, spin state, and centrosymmetry of the site.[13–17] On the other hand, the rising-edge region can give information about geometric structure, metal-ligand overlap, ligand arrangement, and charge on the metal center.[2,18–22] Recently, XANES has been used to interpret covalency of actinide complexes.[23]

Among the many applications of XANES, it has been used as an informative *operando* technique to study supported metal cluster catalysts in reaction conditions.[24–29] In the interpretation of these XANES spectra, the bulk metal and metal oxide standards are used for fitting, in order to extract the average oxidation state of the metal in the cluster. However, it has been recently shown that metal clusters in the subnano regime can be highly fluxional, and that an ensemble of many thermally-accessible isomers rather than one stationary global minimum structure is present in the reaction conditions.[30–38] These minima may differ not only by shape, but also by chemical composition, such as oxygen content in reaction conditions. This complication inevitably puts in question the usual practice of interpreting the *operando* XANES spectra for cluster catalysts. In fact, some aspects of this practice have been challenged already. Anderson et al.[39] have shown that there is a shift toward higher energies in the Pt $L_3$ edge of $Pt_{24}/SiO_2$ relative to the bulk Pt which, at first glance, might be attributed to the increase in the oxidation state of the cluster. However, additional analysis of the oxidation state obtained from X-ray photoelectron spectroscopy (XPS) shows that the shift is due to the inherent size effects in the nano regime rather than change in the oxidation state of Pt. In addition, Bare and co-workers elucidated the structure and dynamics of $PtSn/Al_2O_3$ nanoclusters under working conditions by combining X-ray absorption spectroscopy and ab initio molecular dynamics.[29] Furthermore, molecular dynamics simulation has been used to generate X-ray absorption fine structure (XAFS) spectra by generating a trajectory of the fully

equilibrated chemical system also known as the statistic ensemble of the system.[40] For each snapshot in the trajectory, XAFS is calculated for the atom(s) of interest until an ensemble average spectrum is built based on the contributions from all of the structural information in the ensemble. We should note that this technique has been mainly used to characterize the structure of solvent molecules (mainly water) surrounding various metal complexes, cations, and anions in a solution,[41–50] or at interface.[51] In situ XAFS along with NMR have also been used to investigate dehydrogenation of dimethylamine borane catalyzed by Rhodium based complex under working condition.[52]

Here, we study small supported, partially oxidized Cu clusters, and focus on the Cu K-edge in XANES.[6,11,53] We show that caution is necessary when interpreting the experimental *operando* XANES data for structurally fluxional nanoclusters. One extreme example is $Cu_5O_5$/UNCD, which has numerous isomers with significantly different geometries that can be present at the interface simultaneously, at high temperatures. In the case of $Cu_4O_x/Al_2O_3$, the specific binding to the support also non-trivially influences the XANES signal. Overall, due to the sensitivity of XANES to the geometry of the environment surrounding the metal center, the influence of the support on the cluster, and the inherent size effect in this regime, the apparent oxidation state derived from the experimental spectra should be (i) ensemble-averaged over multiple thermally-accessible structures, and (ii) not directly mapped on the chemical composition. We show that fitting to bulk standards does not provide reliable compositions for these nanoscale clusters. Instead, fitting the experimental XANES to a group of computed XANES spectra of clusters with different compositions gives a much more accurate information about the chemical composition of the dominant cluster in reaction conditions. From these fittings, we derive the compositional change of partially oxidized supported Cu clusters at varying temperatures.

## Experimental Methods

The experimental spectra for the $Cu_5O_x$/UNCD were taken from Ref. 79. For the alumina supported systems, the Cu cluster samples were prepared in a magnetron sputtering source housed in a high-vacuum chamber.[54,55] Thereafter, clusters of 4-atoms were selected using an ion guide assembly[55] and softly landed on the substrate with impact energy lower than 1 eV per atom. This

ensures that clusters do not undergo fragmentation upon landing.[56,57] The substrates were prepared by atomic layer deposition (ALD) of alumina on top of a native oxide of a Si wafer.[55] The cluster surface coverage is maintained as low as 10% of atomic monolayer equivalent, covering two spots of 8 mm diameter. GISAXS (Grazing Incidence Small Angle X-ray Scattering) data show no cluster agglomeration occurring at higher temperatures (see Fig. S4).

The cluster samples were exposed to a gas mixture containing 2% propane and 2% of oxygen in helium under a pressure of 1.1 atm. The samples were heated up to 773 K, and XANES spectra were collected at the Cu K-edge (8.976 keV) at several intermediate temperatures.[58]

## Computational Methods

All $Cu_5O_5$/UNCD and $Cu_5O_3$/UNCD local minima geometries were obtained with plane wave density functional theory calculations implemented in Vienna Ab initio Simulation Package (VASP)[59–62] using projector augmented wave (PAW) potentials[63] and the PBE[64] functional. For the geometry optimizations, kinetic energy cutoffs of 400.0 eV and convergence criteria of $10^{-5}$ ($10^{-6}$) eV for geometric (electronic) relaxations were employed. In addition, Gaussian smearing with the sigma value of 0.1 eV was used. The UNCD surface is represented by a slab model, which was grown from a diamond unit cell with the experimental lattice constant a = 3.5668 Å to a (4 x 4) support with the (100) facet exposed and separated by a vacuum gap of >14 Å along the z direction.[65] A 2 x 2 x 1 Monkhorst-Pack k-point grid was utilized for all UNCD calculations. During calculations, the bottom two carbon layers were kept fixed and terminal hydrogens were applied to both the top and bottom of the surfaces. The cut-off energy of 0.4 eV was used in order to choose the thermodynamically accessible isomers at relevant temperatures. Note that in order to produce the initial cluster geometries on the surface we use our in-house code, parallel global optimization and pathway toolkit (PGOPT), which automatically generates these structures based on the bond length distribution algorithm (BLDA).[66] Initial structures for the global optimization should be created wisely, i.e. in such a way that they are less prone to suffer from a Self-Consistent Field (SCF) convergence problem. By avoiding chemically unfavorable configurations, the configuration search space will be reduced which results in the reduction of computational cost One way to do so is by restricting the distance of atoms to their closest and second closest atoms to follow a normal distribution. In other words, both distances are fitted to normal distribution

based on which the initial structures are generated. This generation algorithm based on the statistical restriction is called BLDA. This algorithm has been extensively used to sample surface supported metal cluster geometries and compared to experimental results and other algorithms such as Basin Hopping.[33,35,36,38,66–71] Then each structure was optimized using DFT calculation and duplicates were removed. The amorphous $Al_2O_3$–supported $Cu_4O_x$ clusters used in this manuscript were obtained by an in-house implemented grand canonical basin hopping method. The details are presented in another paper,[72] and currently exploited structures refer to the optimized stable configurations/stoichiometries under 200 ˚C and 0.5 bar of $O_2$ gas phase. We use the model from a previous paper of Cheng et al.[73] in order to represent amorphous alumina support. The structure optimizations were conducted at the level of DFT with PBE functional being corrected by the Dudarev's scheme[74] of on-site Coulomb interaction ($U - J = 2.0\,eV$) for the $d$ orbitals of Cu atoms. Spin-polarized calculations were used, and the energy cutoff for plane waves basis sets is 400 eV.

The XANES spectra were calculated using the finite difference method (FDM) and Hedin–Lundqvist exchange-correlation potential implemented in Finite Difference Method Near Edge Structure (FDMNES) ab initio package.[75,76] FDMNES, both for molecular and periodic systems, works in real space. The code builds clusters around the absorbing atoms of interest by reading in a radius specified by the user. Then it preforms several independent calculations for non-equivalent absorbing atoms. The radius of calculated cluster in this study in order to compute Cu K-edge spectra of $Cu_4O_x/Al_2O_3$(x = 2–5) and $Cu_5O_y$/UNCD(y = 3, 5) is 7 Å. Once the potential is defined and constructed, the Schrödinger's equation is discretized, i.e. the Laplacian is replaced by a fourth-order polynomial and solved on a discrete lattice. This procedure is done self-consistently to improve the initial constructed potential. This has a significant advantage over the muffin-tin approximation in which it is assumed that the potential in the interstitial regions is constant. We should note that in order to calculate the potential at the border of the defined cluster properly the cluster is embedded in a wider cluster.[77] After that, the contributions of different absorbing atoms in the system are added together. Lastly, the normalization of the spectra and linear combination fitting (LCF) were all done using the Athena software.[78] Linear combination fitting was done around –10 to 30 eV of the main peak.

## Results and Discussion

Figures 1(a) and (b) show the experimental[6] and computed Cu K-edge XANES of bulk Cu, CuO, and $Cu_2O$. As can be seen, there is an increase in the energy corresponding to both the rising-edge and the white line peaks as the oxidation state of copper increases. Note that there is a low-intensity pre-edge peak in the computed CuO spectrum stemming from the 1s to 3d orbital transition, which is usually hard to obtain from the experiment since it is a dipole forbidden but quadruple allowed transition. Both theory and experiment indicate that in the bulk Cu K-edge XANES the rising-edge and the white line maxima shift to higher energies as the Cu oxidation state increases.

The XANES spectra corresponding to the three lowest energy isomers of $Cu_5O_5$/UNCD and $Cu_5O_3$/UNCD, which are within 0.4 eV of the global minimum,[79] are shown in Figure 1(c) and (d). The corresponding cluster geometries (A-C) along with their Boltzmann probabilities of being populated at 535 K (temperature of specific selectivity in oxidative dehydrogenation of cyclohexane catalyzed by these clusters),[38–41] are shown in Figure 3(a). It is clear that the shapes of the XANES spectra, e.g. the positions of the peaks, depend significantly on the cluster geometry. For instance, the position of the rising-edge peaks can vary by more than 4 eV from one isomer to another, for both $Cu_5O_5$/UNCD and $Cu_5O_3$/UNCD. This is actually not unexpected, since XANES is sensitive to the geometry around the metal center, and geometries of the minima differ significantly, from more open and upright, to closed and globular (Figure 3(a)).

At reaction temperatures (535–550 K in this case), the populated minima of the cluster with different geometries will contribute, as weighted by their populations, to the experimental spectra. Hence, the *operando* XANES measures an ensemble-averaged signal. The relative size of the ensemble, and the prevalence of the global minimum in the ensemble are non-trivially system-dependent. For example, for $Cu_5O_3$/UNCD, the global minimum heavily dominates, whereas for $Cu_5O_5$/UNCD it constitutes only 77% of the population at 535 K. The calculated averaged spectra of both systems in Figure 1(c) and (d) should correspond to the experiment more closely than the spectra of individual isomers or the global minimum alone. The effect of higher-energy isomers on XANES is especially pronounced when the ensemble is not dominated by the global minimum structure.

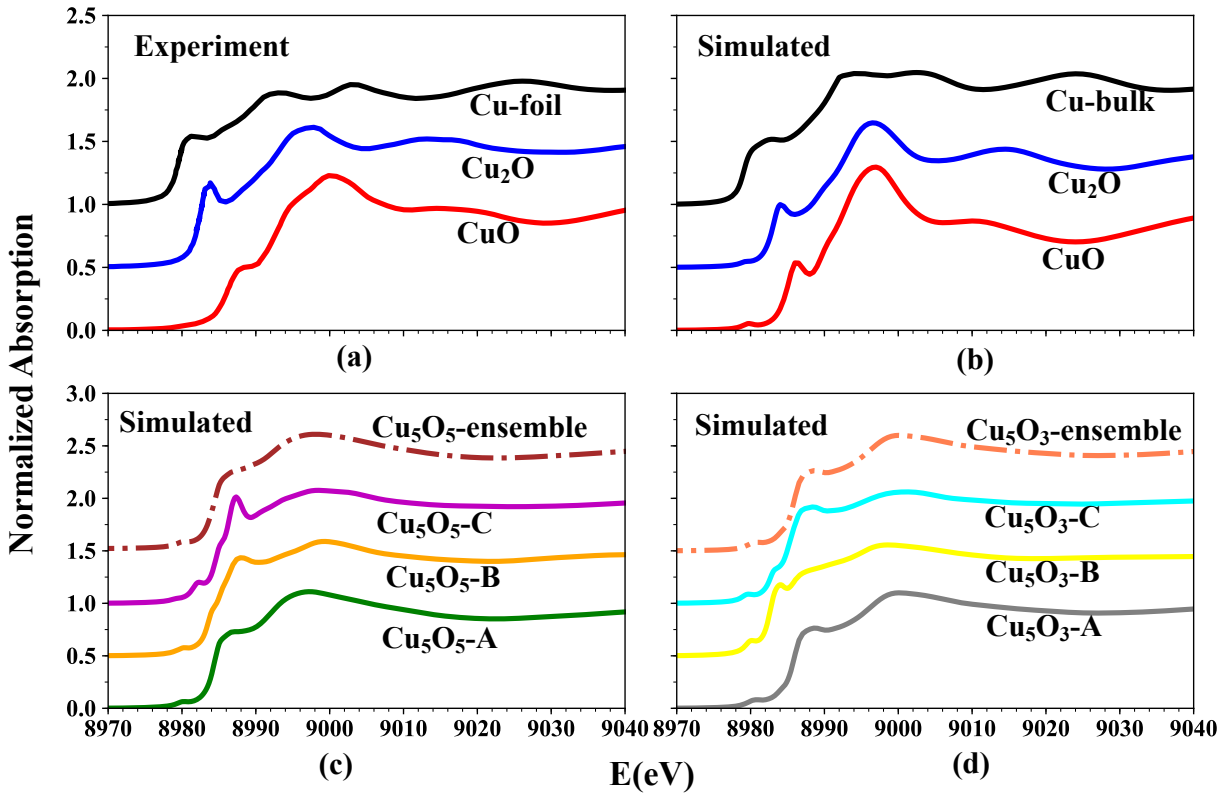


**Figure 1.** (a) Experimental and(b) simulated XANES spectra of bulk Cu, CuO, and $Cu_2O$.(c) Simulated XANES corresponding to the three lowest energy isomers (A, B, and C) of $Cu_5O_5$/UNCD and (d) $Cu_5O_3$/UNCD obtained from global optimization. Note the noticeable difference between the shape of the spectrum even within the same chemical composition. All spectra are stacked vertically for clarity.Experimental spectra were reproduced with permission from refs. [6] and [79].

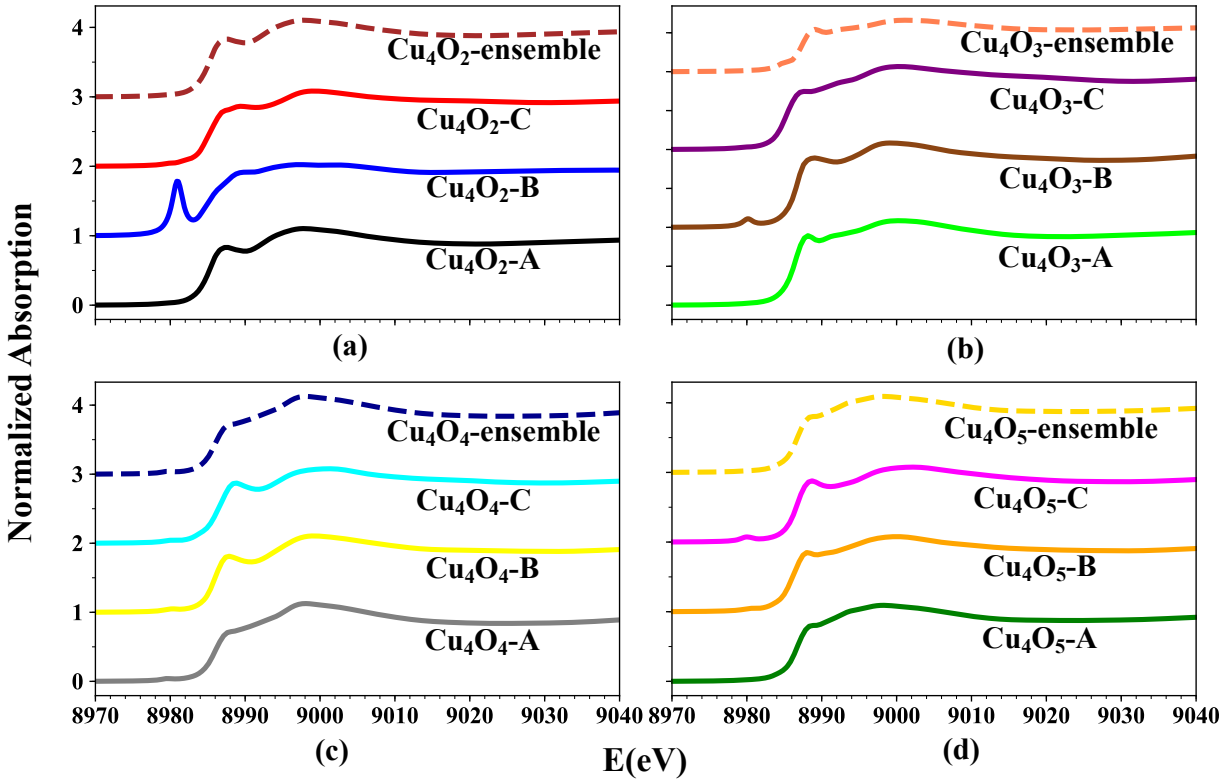


**Figure 2.** Simulated XANES spectra of the three different isomers of $Cu_4O_x/Al_2O_3$ (x = 2–5) obtained from global optimization. Note the noticeable difference between the shape of the spectrum even within the same chemical composition. All spectra are stacked vertically for clarity.

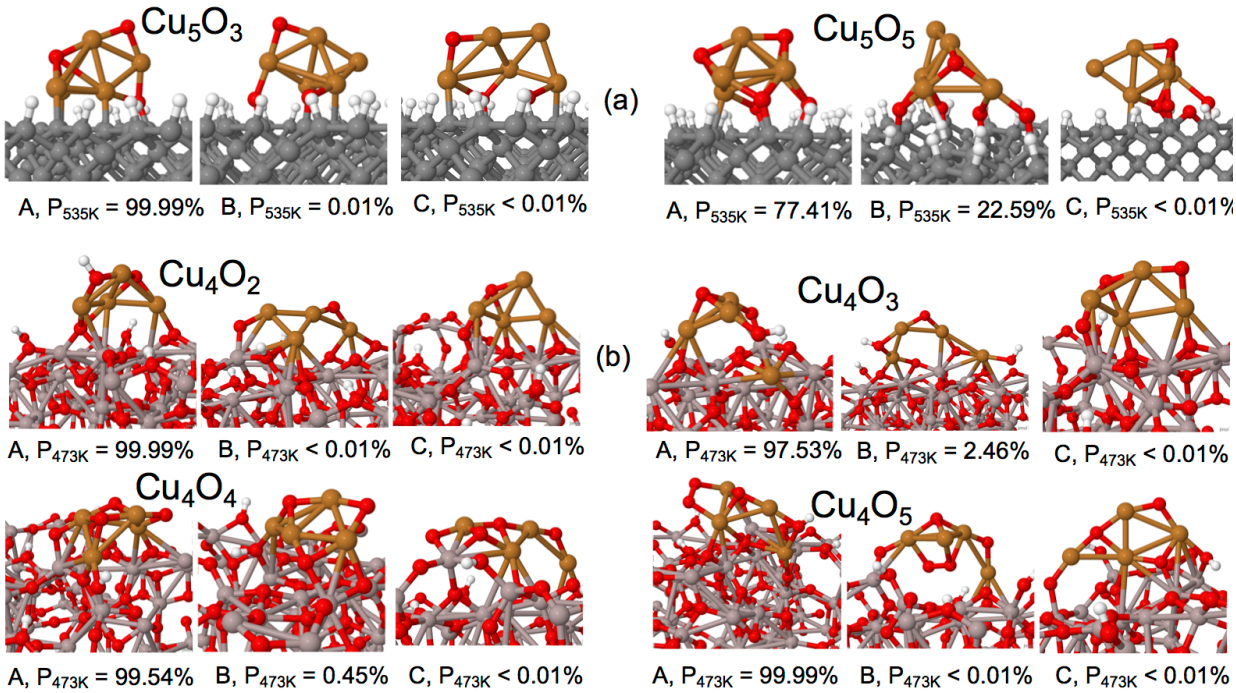


**Figure 3.** (a) Local minimum structures of $Cu_5O_3$/UNCD and $Cu_5O_5$/UNCD obtained from global optimization, along with their corresponding Boltzmann populations calculated at 535 K. (b)Local minimum structures of $Cu_4O_x/Al_2O_3$ (x = 2–5) obtained from grand canonical ensemble optimization at 473 K and $p_{O2}$ = 0.5 bar. Note that for every composition of $Cu_4O_x/Al_2O_3$ (x = 2–5) the three lowest energy isomers with significantly different geometries, thus noticeable different XANES, were chosen.

Do the spectra correlate with the oxygen content, the hallmark of oxidation? All the energies corresponding to the rising-edge and K-edge peak of the bulk Cu, $Cu_2O$, and CuO, and $Cu_5O_3$/UNCD, $Cu_5O_5$/UNCD, and $Cu_4O_x/Al_2O_3$ (x = 2–5) obtained from our calculations are depicted in Figure 4 with their values summarized in detail in Table S1. Comparing the spectra of the global minima of the more oxidized $Cu_5O_5$-A/UNCD (green), and the partially reduced $Cu_5O_3$-A/UNCD (gray) (Figure 1(d)), one can see that the trend is the opposite of what is found for the oxidized and reduced bulk Cu systems (Figure 4). From the calculated and experimental spectra of the bulk, $Cu_5O_5$/UNCD is expected to have higher $E_{rising\text{-}edge}$ and $E_{white\text{-}line}$ than those of$Cu_5O_3$/UNCD, but we find this not to be the case. For the bulk calculations there is a 3 eV increase in both the rising-edge and white line energies as the oxidation state increases, while there is a 3 eV decrease in the white line energy when comparing the global minimum structures of $Cu_5O_3$/UNCD and $Cu_5O_5$/UNCD.

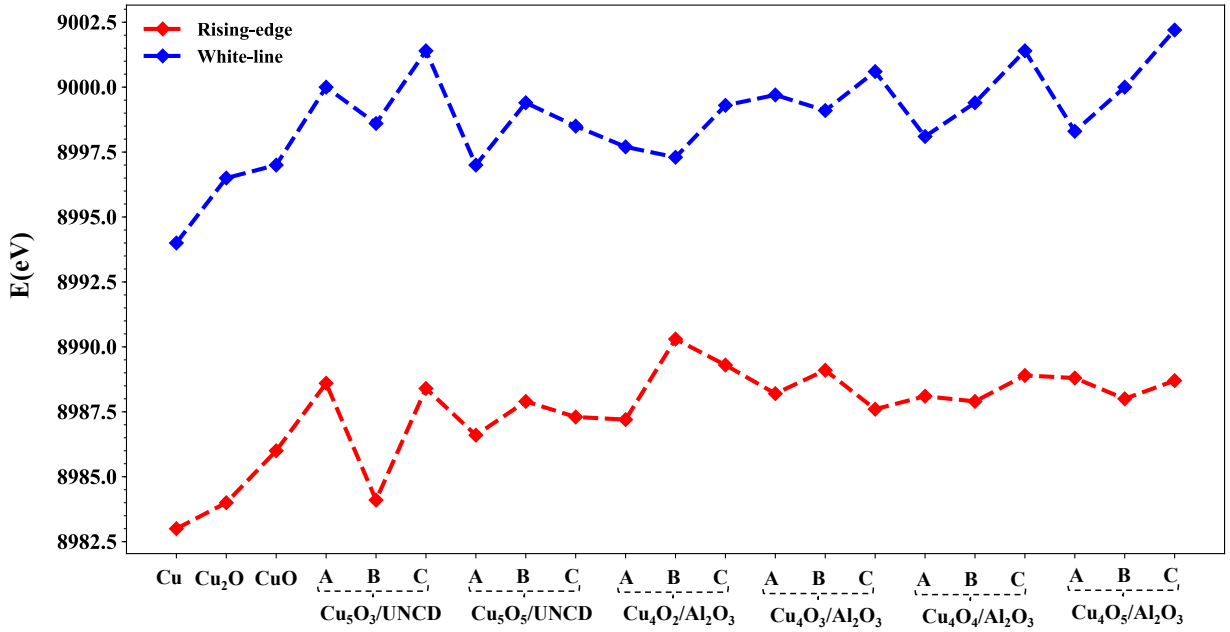


**Figure 4.** Calculated $E_{rising\text{-}edge}$(in red) and $E_{white\text{-}line}$(in blue) peaks corresponding to the bulk Cu, $Cu_2O$, CuO, and all of the surface-supported isomers of $Cu_5O_3$/UNCD, $Cu_5O_5$/UNCD, and $Cu_4O_x/Al_2O_3$ (x = 2–5) explored in this letter. It is clear that clusters do not necessarily follow the bulk trend.

The global minimum structure alone is an insufficient model of the catalytic system, as we emphasized in the past.[30–38] It is clear from Table S1 and Figure 4 that the position of the rising-edge and white line peaks from one isomer to another for the cluster of the same composition can vary up to 4.5 eV and 2.4 eV, respectively (compare $E_{rising\text{-}edge}$ of $Cu_5O_3$-A and $Cu_5O_5$-B, and $E_{white\text{-}line}$ of $Cu_5O_5$-A and $Cu_5O_5$-B). As a result, some of the $Cu_5O_3$/UNCD isomers have higher $E_{rising\text{-}edge}$ and/or $E_{white\text{-}line}$ than some of the $Cu_5O_5$/UNCD isomers, while others have the opposite trend. For instance, $E_{rising\text{-}edge}$ and $E_{white\text{-}line}$ of $Cu_5O_3$-A are higher than those of $Cu_5O_5$-A, whereas $Cu_5O_3$-B has lower $E_{rising\text{-}edge}$ and $E_{white\text{-}line}$ than those of $Cu_5O_5$-B. Note that, beyond the representation of the cluster as a statistical ensemble of minima, an additional effect may arise due to thermal fluctuations within each minimum, which can be captured by *ab initio* MD. For example, Bare and Rehr and co-workers showed what effect thermal smearing could have on the computed XANES.[29] In the end, correlating the shape of the *operando* XANES spectrum and positions of the peaks, and the average oxidation state of the metal in the cluster is far from straightforward.

Besides the oxygen content, the electron transfer between the support and the cluster can affect the oxidation state of Cu. Our calculations show that UNCD has a relatively low work function (3.35 eV, Figure S1) and thus easily gives electrons to the metal oxide clusters. Note that the experimental value of the work function is 3.3 eV for nanocrystalline diamond,[83] and 3.6 eV for nitrogen-doped UNCD.[84] The Bader charge analysis shows that the total charge on the cluster in $Cu_5O_3$/UNCD and $Cu_5O_5$/UNCD can be up to –1.69 e and –3.50 e respectively with the charge on Cu varying from –0.14 e to 0.76 e.[79] Bader charge analysis shows that the average charge of Cu in the $Cu_5O_3$ isomers is 0.49 e, 0.28 e, and 0.26 e, and in the $Cu_5O_5$ isomers it is 0.62 e, 0.38 e, and 0.35 e respectively. This shows an increase in the average charge of Cu, which is expected but does not necessarily correlate with information obtained from XANES.

Next, we probed a different support (amorphous alumina), and a broader set of CuO cluster stoichiometries, to check if our conclusions are not confined to the specific chemistry of the system. Figure 2 shows the calculated XANES spectra of the $Cu_4O_x/Al_2O_3$ (x = 2–5) clusters. These species are the three lowest energy isomers identified through grand canonical global optimization(on the quasi free energy surface) in conditions of 0.5 bar $O_2$ and 200 ˚C, corresponding to oxidative dehydrogenation of propane.[72,79,85] The isomers differ in oxygen content and have significantly different geometries for each cluster composition (see Figure 3(b)).The XANES spectra in this case are intensely dependent on the cluster isomers. First of all, since in this case the support itself contains oxygen, and there is a known tendency of copper to mix with alumina to form copper aluminate,[86–88] the oxygen content of the cluster might be vague to define. In other words, Cu binds to the support and may partially dissolve in it, making it hard to define the stoichiometry of the supported cluster itself. The oxygen of the support can influence the charge on the metal in the cluster and affect the XANES spectrum correspondingly. This shows the importance of the nature of the support and how it can affect the shape of the spectrum. Furthermore, since the support is amorphous alumina, hydrogen atoms from the hydroxyl groups present in the support can migrate to the oxygen in the cluster and affect the charge state of the copper. Such structures with spontaneous H reverse spill-over have been seen in the global optimization, e.g. isomer C of $Cu_4O_5$ on alumina (Figure 3(b)). Such events can significantly modify the shapes of the XANES spectra.

In the isomer $Cu_4O_2$-B, there is an intense pre-edge peak, which stems from the transition of 1s electron to the p component in d–p hybridized orbitals. Itis not unprecedented. The transition of a 1s electron to a d–p hybridized orbital consists of the electric quadrupole transition to the d-character component and the electric dipole transition to the p-character component. Here an intense pre-edge peak of almost fully occupied Cu d orbitals consists mainly of the large dipole transitions to the p-character component. Additionally, the highly asymmetric structure of $Cu_4O_2$-B leads to broken inversion symmetry, and the average Cu-Cu bond distance is ~0.3 Å shorter than in other $Cu_4O_2$ clusters. Similar intense pre-edge peaks have been reported before for the K-edge of Cu in $(HC[C(Me)NAr]_2)Cu(\eta^2\text{-}PhCH{=}CH_2)$,[14] Mn in $KMnO_4$,[89–92] Ti in $Ba_2TiO_4$, $K_6Ti_2O_7$ and $Rb_2TiO_3$,[93,94] and Ni in $K_2Ni(CN)_4.2H_2O$.[95]

We also investigated the effect of the varying Hubbard *U* correction within DFT on the shape of the XANES spectra (see Figure S2). For $Cu_5O_3$/UNCD, in general, there is no significant change in the rising-edge peak of the spectrum after adding Hubbard *U* to the calculation, while the pre-edge peak gets sharper up until $U = 5$ eV, and decreases afterwards. On the other hand, the rising edge shoulder in the $Cu_5O_5$/UNCD spectrum slowly converts to a noticeable peak as the value of *U* increases, while the pre-edge peak vanishes. In general, the changes are insignificant and do not affect the overall conclusions of this work.

Finally, we performed linear combination fitting (LCF) of calculated XANES of clusters with respect to the bulk XANES, to assess whether or not the bulk standards are a reliable reference for surface-supported fluxional clusters. The obtained coefficients of $Cu_2O$ and CuO show the contribution of each bulk spectrum to the LCF of each cluster spectrum, as seen in Figure 5 and summarized in Table S2. It is clear from Figure 5 that LCF to the bulk spectra does not reliably correlate with the oxygen content in the cluster. For example, the fitting shows $C_{Cu2O} < C_{CuO}$ for $Cu_5O_3$-A and $C_{Cu2O} > C_{CuO}$ for $Cu_5O_5$-A while the opposite trend is, of course, expected. Note as well that $Cu_5O_3$-A and $Cu_5O_5$-A differ not only by the oxygen content, but also by the calculated average charge of Cu, which is larger in $Cu_5O_5$ than in $Cu_5O_3$.[79] In addition, in some cases, fitting to the bulk standards fails completely for these clusters. For instance, for $Cu_5O_3$-B, despite our many attempts with different initial guesses for the coefficients, the fitting procedure fails to properly fit to both $Cu_2O$ and CuO bulk spectra. When it comes to $Cu_4O_x/Al_2O_3$ (x = 2–5), we see less significant of a problem with LCF. In this case, $C_{CuO}$ increases as the number of O increase in

the cluster for the global minimum structures (A structures), as expected. However, if we look at other isomers, there is no monotonous increase or decrease in $C_{CuO}$ value with the changing O-content, and instead the value of $C_{CuO}$ fluctuates up and down.

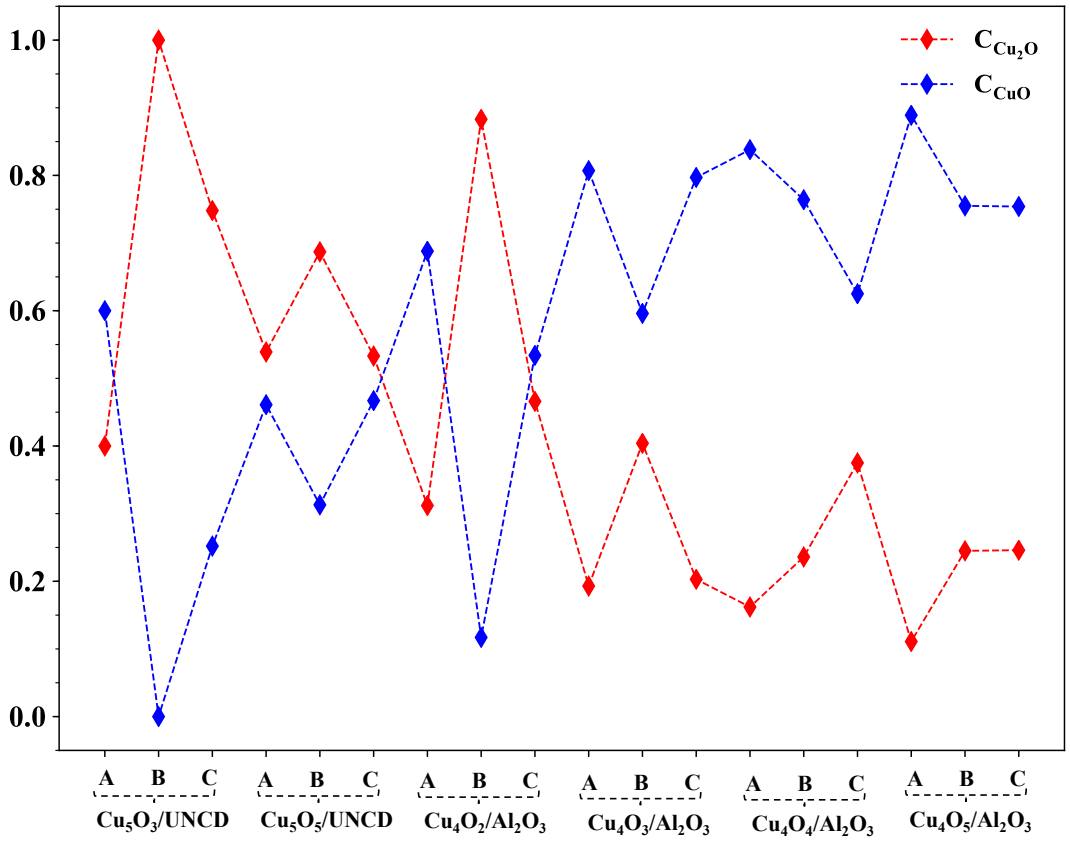


**Figure 5.** $C_{Cu2O}$ and $C_{CuO}$ are the coefficients of $Cu_2O$ and CuO XANES, respectively, obtained from the LCF of XANES of $Cu_5O_5$/UNCD, $Cu_5O_3$/UNCD, and $Cu_4O_x/Al_2O_3$ (x = 2–5). In general, there is no clear correlation between the obtained coefficients and oxygen content of the clusters.

Figure 6 shows the original computed XANES spectra along with the LCF to the bulk for every supported cluster in this study. Although in some cases LCF captures the peaks qualitatively, it does not give a decent quantitative position of the peaks, especially in the rising edge area. This difference can be more than 5 eV at times, making the LCF of surface-supported clusters to their corresponding bulk structure an unreliable method.

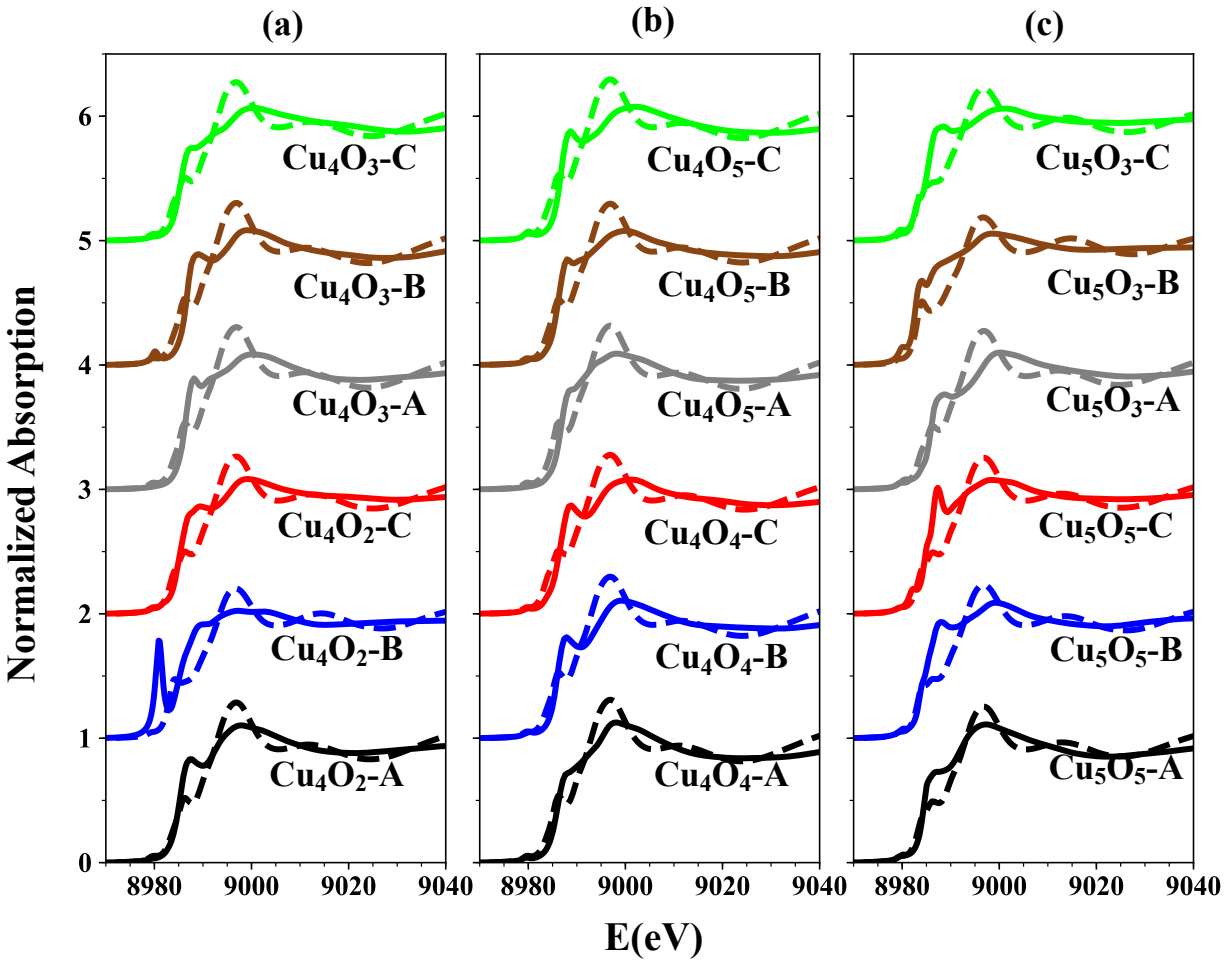


**Figure 6.** Solid curves: XANES spectra corresponding to thermally-accessible isomers of (a) $Cu_4O_x/Al_2O_3$ (x = 2, 3) and (b) $Cu_4O_x/Al_2O_3$ (x = 4, 5), and (c) $Cu_5O_3$/UNCD and $Cu_5O_5$/UNCD. Dashed curves: LCF spectra obtained using the bulk $Cu_2O$ and CuO XANES as references.

We also calculated the ensemble average XANES of UNCD- and $Al_2O_3$-supported CuO clusters. These are more likely to correspond to the *operando* XANES measurements in realistic reaction conditions of $T$ and $p_{O2}$. Figure 7 compares the experimental Cu K-edge XANES of $Cu_4O_x$on amorphous $Al_2O_3$ with the ensemble average XANES, LCF to the bulk CuO and $Cu_2O$, and LCF to the supported clusters at 423 K. Since we showed that using bulk as reference in order to find the chemical composition of clusters is unreliable at times, we tried to use computed XANES of clusters as reference for LCF of the experimental data, to obtain more accurate and detailed information about the composition of the cluster (Figure 7).The cluster "standards" included in the LCF are the global minima of each composition (LCF-cluster$_1$). We also fitted to

other higher-energy minima, again one of each composition, but such that they are significantly different in shapes (LCF-cluster$_2$). Note that since $Cu_4O_x/Al_2O_3$ structures were obtained using grand canonical basin hopping, ensemble average over different composition is possible, whereas $Cu_5O_x$/UNCD (x = 3, 5) structures obtained separately in a canonical ensemble; therefore, here we only discuss $Cu_4O_x/Al_2O_3$ (x = 2–5).Note that since the energies of copper clusters depend on the value of Hubbard $U$, we choose two different values: $U$ = 2 eV where $Cu_4O_3$ is the global minimum, and $U$ = 7 eV where $Cu_4O_4$ is the global minimum structure in the $Cu_4O_x$ (x = 2–5) ensemble.

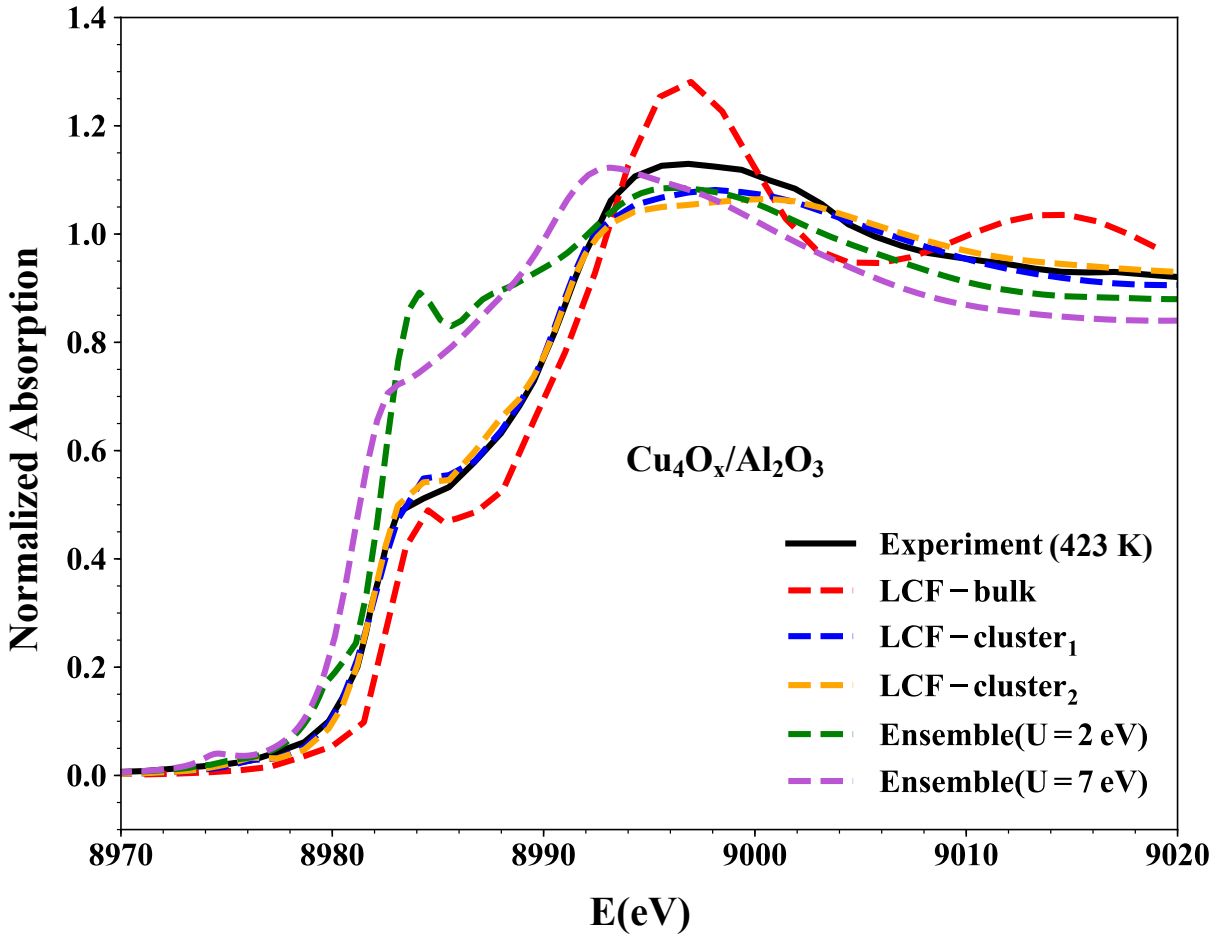


**Figure 7.** Experimental Cu K-edge XANES obtained at 423 K along with the ensemble average over $Cu_4O_x/Al_2O_3$ (x = 2–5), LCF to the bulk, and LCF to the computed XANES of the global minima for

different O content (LCF-cluster$_1$) and higher-energy minima (LCF-cluster$_2$) of $Cu_4O_x/Al_2O_3$ (x = 2–5) used as reference.

As can be seen, LCF to the cluster "standards" obviously fits the experiment better (See blue and red curves in Figure 7). The obtained R-factor, which is a measure of mean square sum of the misfit at each data point, is 0.0028, 0.0046, and 0.1178, for LCF-cluster$_1$, LCF-cluster$_2$, and LCF-bulk, respectively. More importantly, TheLCF-cluster$_1$ gives the following composition: 15.4% $Cu_4O_2$, 0.0% $Cu_4O_3$, 49.9% $Cu_4O_4$, and 34.7% $Cu_4O_5$, suggesting that the dominant chemical composition of $Cu_4O_x/Al_2O_3$ at reaction temperature is $Cu_4O_4$ followed by a mixture of $Cu_4O_5$and $Cu_4O_2$. However, fitting to the bulk yields 74.5% $Cu_2O$ and 24.5%CuO which is the opposite of what the LCF-cluster$_1$ suggests. Interestingly, fitting to non-global minima of all compositions gives qualitatively similar results. The composition obtained from LCF-cluster$_2$is 0.0% $Cu_4O_2$, 19.0% $Cu_4O_3$, 60.1% $Cu_4O_4$, and 20.9% $Cu_4O_5$, again suggesting $Cu_4O_4$ as the dominant composition but followed by $Cu_4O_5$ and $Cu_4O_3$. Hence, LCF to the bulk in this case will be misleading and questionable, and LCF to the cluster should be used instead. Note that Boltzmann populations obtained from grand canonical ensemble can be dependent on the value of the *U* parameter used in the global optimization method, thus affecting the shape of the ensemble-averaged XANES; however, the obtained structures can be used as "standards" for LCF-cluster in order to obtain more accurate information about the composition of the cluster in reaction condition.

Figure 8 shows the obtained coefficients of $Cu_4O_x/Al_2O_3$ (x = 2–5) clusters when fitted to the experimental XANES as a function of temperature. It is clear that there is a reduction in the Cu cluster oxidation state at high temperature: the dominant cluster composition changes from $Cu_4O_4$ at 423 K to $Cu_4O_2$ at 773 K. All values are summarized in Table S3. Furthermore, Figure S3 shows the experimental XANES along with their corresponding LCF spectrum at 423 K, 673 K, and 773 K.

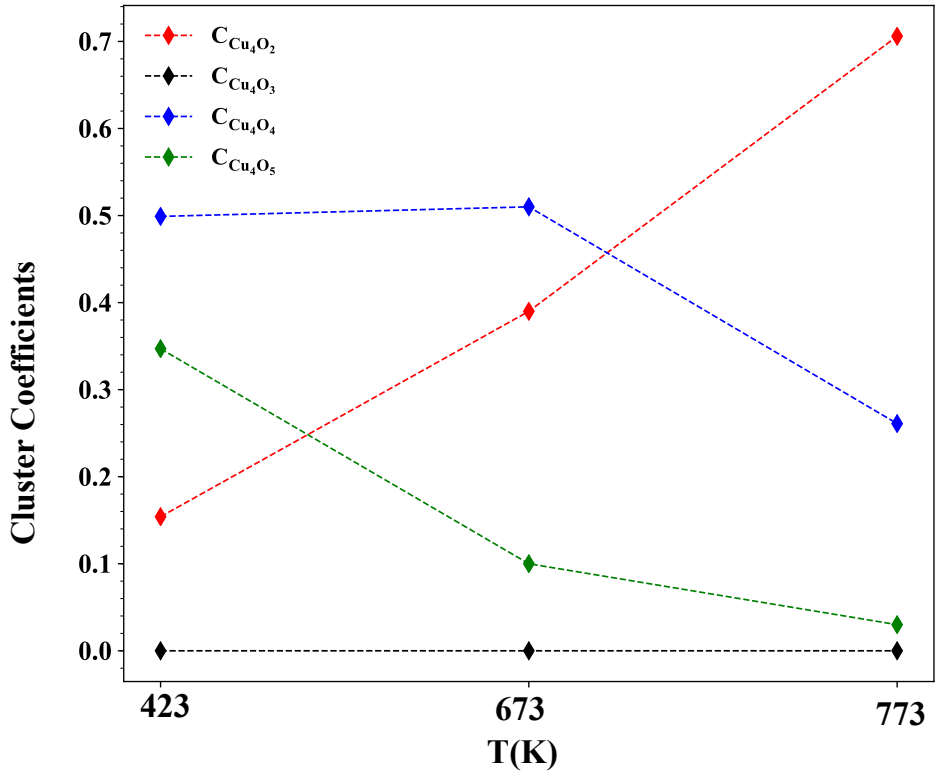


**Figure 8.** Obtained coefficients of $Cu_4O_x/Al_2O_3$ (x = 2–5) from LCF to the experimental XANES at three different temperatures. $Cu_4O_2$ becomes dominant at high temperature showing a reduction in the cluster oxidation state.

## Conclusions

To summarize, we have shown that analyzing XANES spectra of surface-supported clusters in the non-scalable regime using the bulk standards is inaccurate. By comparing both experimental and theoretical Cu K-edge XANES we found that, in addition to the inherent cluster size effect, the presence of numerous isomers in reaction conditions can affect the XANES spectra. Isomers can be significantly different in their geometric and electronic structures, amount of charge transfer from the support, as well as oxygen content. The resultant XANES do not map onto the bulk standards in a predictable manner. Therefore, one has to take into account the importance of fluxionality and size effect when interpreting XANES of surface-supported nanoclusters. We additionally conclude that the stoichiometry of these clusters in reaction conditions cannot be derived from the corresponding bulk XANES and has to be obtained by other means. We propose that LCF to the computationally obtained cluster "standards" could be a more

reliable approach to determining cluster compositions in reaction conditions. Using this approach, we conclude that oxidized Cu clusters undergo partial reduction at temperatures typical for oxidative dehydrogenation of alkanes.

## ASSOCIATED CONTENT

Supporting Information Available: UNCD work function plot, the effect of Hubbard *U* on the XANES spectra, Tables containing $E_{rising\text{-}edge}$, $E_{white\text{-}line}$, and LCF coefficients of all supported clusters in this study. Note that the XYZ coordinates of all structures used in this study can be found here: https://github.com/bzkarimi/xanes-structs.

## AUTHOR INFORMATION


### ORCIDs

Borna Zandkarimi: 0000-0002-7633-132X

Avik Halder: 0000-0002-9775-0558

Soenke Seifert: 0000-0003-4598-2354

Stefan Vajda: 0000-0002-1879-2099

Philippe Sautet: 0000-0002-8444-3348

Anastassia Alexandrova: 0000-0002-3003-1911


### Notes

The authors declare no competing financial interest.

## ACKNOWLEDGEMENT

The theoretical part of this work was funded by DOE-BES grant DE-SC0019152. CPU resources at the Extreme Science and Engineering Discovery Environment's (XSEDE) computing resources were used. The work at Argonne (A.H., S.V.) was supported by the US Department of Energy, BES Materials Sciences under Contract DEAC02–06CH11357 with University of Chicago Argonne, LLC, operator of Argonne National Laboratory, the work at the Advance Photon Source (S.S., beamline 12-ID-C) by the US DOE, Scientific User Facilities under Contract DEAC02-06CH11357.The authors thank Dr. Michael Pellin for providing the alumina-coated wafers. S.V. also acknowledges support from the European Union's Horizon 2020 research and innovation program under grant agreement No 810310, which corresponds to the J. Heyrovsky Chair project ("ERA Chair at J. Heyrovský Institute of Physical Chemistry AS CR – The institutional approach towards ERA") during the finalization of the paper. The funders had no role in the preparation of the article.

## REFERENCES

(1) Norman, D. X-Ray Absorption Spectroscopy (Exafs and Xanes) at Surfaces. *J. Phys. C Solid State Phys.* **1986**, *19*, 3273–3311.

(2) Rehr, J. J.; Ankudinov, A. L. Progress in the Theory and Interpretation of XANES. *Coord. Chem. Rev.* **2005**, *249*, 131–140.

(3) Henderson, G. S.; de Groot, F. M. F.; Moulton, B. J. A. X-Ray Absorption Near-Edge Structure (XANES) Spectroscopy. *Rev. Mineral. Geochemistry* **2014**, *78*, 75–138.

(4) Larsson, M.; Lindén, J. B.; Kaur, S.; Le Cerf, B.; Kempson, I. Cu K-Edge XANES: Polymer, Organic, Inorganic Spectra, and Experimental Considerations. *Powder Diffr.* **2017**, *32*, S28–S32.

(5) Zhang, R.; McEwen, J. S. Local Environment Sensitivity of the Cu K-Edge XANES Features in Cu-SSZ-13: Analysis from First-Principles. *J. Phys. Chem. Lett.* **2018**, *9*, 3035–3042.

(6) Gaur, A.; Shrivastava, D.; Joshi, K. Copper K-Edge XANES of Cu(I) and Cu(II) Oxide Mixtures. *J. Phys. Conf. Ser.* **2009**, *190*, 012084–012088.

(7) Korzhavyi, P. A.; Johansson, B. Literature Review on the Properties of Cuprous Oxide $Cu_2O$ and the Process of Copper Oxidation; Svensk Kärnbränslehantering AB, SKB TR-11-08, Stockholm, Sweden, **2011**.

(8) Timoshenko, J.; Halder, A.; Yang, B.; Seifert, S.; Pellin, M. J.; Vajda, S.; Frenkel, A. I. Subnanometer Substructures in Nanoassemblies Formed from Clusters under a Reactive Atmosphere Revealed Using Machine Learning. *J. Phys. Chem. C* **2018**, *122*, 21686–21693.

(9) Solomon, E. I.; Hedman, B.; Hodgson, K. O.; Dey, A.; Szilagyi, R. K. Ligand K-Edge X-Ray Absorption Spectroscopy: Covalency of Ligand–Metal Bonds. *Coord. Chem. Rev.* **2005**, *249*, 97–129.

(10) Mammen, N.; Spanu, L.; Tyo, E. C.; Yang, B.; Halder, A.; Seifert, S.; Pellin, M. J.; Vajda, S.; Narasimhan, S. Reversing Size-Dependent Trends in the Oxidation of Copper Clusters through Support Effects. *Eur. J. Inorg. Chem.* **2018**, *2018*, 16-–22.

(11) Mammen, N.; Spanu, L.; Tyo, E. C.; Yang, B.; Halder, A.; Seifert, S.; Pellin, M. J.; Vajda, S.; Narasimhan, S. Using First Principles Calculations to Interpret XANES Experiments: Extracting the Size-Dependence of the (p, T) Phase Diagram of Sub-Nanometer Cu Clusters in an $O_2$ Environment. *J. Phys. Condens. Matter* **2019**, *31*, 144002–144012.

(12) Wilke, M.; Hahn, O.; Woodland, A. B.; Rickers, K. The Oxidation State of Iron Determined by Fe K-Edge XANES -Application to Iron Gall Ink in Historical Manuscripts. *J. Anal. At. Spectrom.* **2009**, *24*, 1364–1372.

(13) De Groot, F.; Vankó, G.; Glatzel, P. The 1s X-Ray Absorption Pre-Edge Structures in Transition Metal Oxides. *J. Phys. Condens. Matter* **2009**, *21*, 104207–104213.

(14) Tomson, N. C.; Williams, K. D.; Dai, X.; Sproules, S.; DeBeer, S.; Warren, T. H.; Wieghardt, K. Re-Evaluating the Cu K Pre-Edge XAS Transition in Complexes with Covalent Metal-Ligand Interactions. *Chem. Sci.* **2015**, *6*, 2474–2487.

(15) James, C. Structural Techniques. In Structural Chemistry of Glasses; Rao, K. J. Ed.; Elsevier Science Ltd: Oxford, 2002; pp 137–183.

(16) Yamamoto, T. Assignment of Pre-Edge Peaks in K-Edge x-Ray Absorption Spectra of 3d

Transition Metal Compounds: Electric Dipole or Quadrupole? *X-Ray Spectrom.* **2008**, *37*, 572–584.

(17) Westre, T. E.; Kennepohl, P.; DeWitt, J. G.; Hedman, B.; Hodgson, K. O.; Solomon, E. I. A Multiplet Analysis of Fe K-Edge 1s → 3d Pre-Edge Features of Iron Complexes. *J. Am. Chem. Soc.* **1997**, *119*, 6297–6314.

(18) Hall, M. D.; Foran, G. J.; Zhang, M.; Beale, P. J.; Hambley, T. W. XANES Determination of the Platinum Oxidation State Distribution in Cancer Cells Treated with Platinum(IV) Anticancer Agents. *J. Am. Chem. Soc.* **2003**, *125*, 7524–7525.

(19) Zhang, F.; Wang, P.; Koberstein, J.; Khalid, S.; Chan, S.-W. Cerium Oxidation State in Ceria Nanoparticles Studied with X-Ray Photoelectron Spectroscopy and Absorption near Edge Spectroscopy. *Surf. Sci.* **2004**, *563*, 74–82.

(20) Manceau, A.; Marcus, M. A.; Grangeon, S. Determination of Mn Valence States in Mixed-Valent Manganates by XANES Spectroscopy. *Am. Mineral.* **2012**, *97*, 816–827.

(21) Wilke, M.; Farges, F.; Petit, P.-E.; Brown Jr., G. E.; Martin, F. Oxidation State and Coordination of Fe in Minerals: An Fe K-XANES Spectroscopic Study. *Am. Mineral.* **2001**, *86*, 714–730.

(22) Siri, G. J.; Ramallo-López, J. M.; Casella, M. L.; Fierro, J. L. G.; Requejo, F. G.; Ferretti, O. A. XPS and EXAFS Study of Supported PtSn Catalysts Obtained by Surface Organometallic Chemistry on Metals: Application to the Isobutane Dehydrogenation. *Appl. Catal. A Gen.* **2005**, *278*, 239–249.

(23) Sergentu, D.-C.; Duignan, T. J.; Autschbach, J. Ab Initio Study of Covalency in the Ground versus Core-Excited States and X-Ray Absorption Spectra of Actinide Complexes. *J. Phys. Chem. Lett.* **2018**, *9*, 5583–5591.

(24) Whiting, G. T.; Meirer, F.; Weckhuysen, B. M. Operando EXAFS and XANES of Catalytic Solids and Related Materials. In *XAFS Techniques for Catalysts, Nanomaterials, and Surfaces*; Iwasawa, Y., Asakura, K., Tada, M., Eds.; Springer International Publishing: Cham, 2017; pp 167–191.

(25) Guda, A. A.; Guda, S. A.; Lomachenko, K. A.; Soldatov, M. A.; Pankin, I. A.; Soldatov,

A. V; Braglia, L.; Bugaev, A. L.; Martini, A.; Signorile, M.; Groppo, E.; Piovano, A.; Borfecchia, E.; Lamberti, C. Quantitative Structural Determination of Active Sites from in Situ and Operando XANES Spectra: From Standard Ab Initio Simulations to Chemometric and Machine Learning Approaches. *Catal. Today* **2019**, *336*, 3–21.

(26) Nayak, C.; Jain, P.; Vinod, C. P.; Jha, S. N.; Bhattacharyya, D. Operando X-Ray Absorption Spectroscopy Study of the Fischer–Tropsch Reaction with a Co Catalyst. *J. Synchrotron Radiat.* **2019**, *26*, 137–144.

(27) Lamberti, C.; Bordiga, S.; Bonino, F.; Prestipino, C.; Berlier, G.; Capello, L.; D'Acapito, F.; Llabrés i Xamena, F. X.; Zecchina, A. Determination of the Oxidation and Coordination State of Copper on Different Cu-Based Catalysts by XANES Spectroscopy in Situ or in Operando Conditions. *Phys. Chem. Chem. Phys.* **2003**, *5*, 4502–4509.

(28) Yao, S.; Mudiyanselage, K.; Xu, W.; Johnston-Peck, A. C.; Hanson, J. C.; Wu, T.; Stacchiola, D.; Rodriguez, J. A.; Zhao, H.; Beyer, K. A.; Chapman, K. W.; Chupas, P. J.; Martínez-Arias, A.; Si, R.; Bolin, T. B.; Liu, W.; Senanayake, S. D. Unraveling the Dynamic Nature of a $CuO/CeO_2$ Catalyst for CO Oxidation in Operando: A Combined Study of XANES (Fluorescence) and DRIFTS. *ACS Catal.* **2014**, *4*, 1650–1661.

(29) Vila, F. D.; Rehr, J. J.; Kelly, S. D.; Bare, S. R. Operando Effects on the Structure and Dynamics of $Pt_nSn_m/\gamma\text{-}Al_2O_3$ from Ab Initio Molecular Dynamics and X-Ray Absorption Spectra. *J. Phys. Chem. C* **2013**, *117*, 12446–12457.

(30) Zhai, H.; Alexandrova, A. N. Fluxionality of Catalytic Clusters: When It Matters and How to Address It. *ACS Catal.* **2017**, *7*, 1905–1911.

(31) Zandkarimi, B.; Alexandrova, A. N. Surface-supported Cluster Catalysis: Ensembles of Metastable States Run the Show. *Wiley Interdiscip. Rev. Comput. Mol. Sci.* **2019**, *9*, e1420.

(32) Sun, G.; Sautet, P. Metastable Structures in Cluster Catalysis from First-Principles: Structural Ensemble in Reaction Conditions and Metastability Triggered Reactivity. *J. Am. Chem. Soc.* **2018**, *140*, 2812–2820.

(33) Zhai, H.; Alexandrova, A. N. Local Fluxionality of Surface-Deposited Cluster Catalysts:

The Case of $Pt_7$ on $Al_2O_3$. *J. Phys. Chem. Lett.* **2018**, *9*, 1696–1702.

(34) Jimenez-Izal, E.; Alexandrova, A. N. Computational Design of Clusters for Catalysis. *Annu. Rev. Phys. Chem.* **2018**, *69*, 377–400.

(35) Zandkarimi, B.; Alexandrova, A. N. Dynamics of Subnanometer Pt Clusters Can Break the Scaling Relationships in Catalysis. *J. Phys. Chem. Lett.* **2019**, *10*, 460–467.

(36) Jimenez-Izal, E.; Zhai, H.; Liu, J. Y.; Alexandrova, A. N. Nanoalloying MgO-Deposited Pt Clusters with Si to Control the Selectivity of Alkane Dehydrogenation. *ACS Catal.* **2018**, *8*, 8346–8356.

(37) Ha, M. A.; Baxter, E. T.; Cass, A. C.; Anderson, S. L.; Alexandrova, A. N. Boron Switch for Selectivity of Catalytic Dehydrogenation on Size-Selected Pt Clusters on $Al_2O_3$. *J. Am. Chem. Soc.* **2017**, *139*, 11568–11575.

(38) Baxter, E. T.; Ha, M. A.; Cass, A. C.; Alexandrova, A. N.; Anderson, S. L. Ethylene Dehydrogenation on $Pt_{4,7,8}$ Clusters on $Al_2O_3$: Strong Cluster Size Dependence Linked to Preferred Catalyst Morphologies. *ACS Catal.* **2017**, *7*, 3322–3335.

(39) Dai, Y.; Gorey, T. J.; Anderson, S. L.; Lee, S.; Lee, S.; Seifert, S.; Winans, R. E. Inherent Size Effects on XANES of Nanometer Metal Clusters: Size-Selected Platinum Clusters on Silica. *J. Phys. Chem. C* **2017**, *121*, 361–374.

(40) Schenter, G. K.; Fulton, J. L. Molecular Dynamics Simulations and XAFS (MD-XAFS). In XAFS Techniques for Catalysts, Nanomaterials, and Surfaces; Iwasawa, Y., Asakura, K., Tada, M., Eds.; Springer International Publishing: Cham, 2017; pp 251–270.

(41) Campbell, L.; Rehr, J. J.; Schenter, G. K.; McCarthy, M. I.; Dixon, D. XAFS Debye-Waller Factors in Aqueous $Cr^{3+}$ from Molecular Dynamics. *J. Synchrotron Radiat.* **1999**, *6*, 310–312.

(42) Zhuang, D.; Riera, M.; Schenter, G. K.; Fulton, J. L.; Paesani, F. Many-Body Effects Determine the Local Hydration Structure of $Cs^+$ in Solution. *J. Phys. Chem. Lett.* **2019**, *10*, 406–412.

(43) Duignan, T. T.; Schenter, G. K.; Fulton, J. L.; Huthwelker, T.; Balasubramanian, M.;

Galib, M.; Baer, M. D.; Wilhelm, J.; Hutter, J.; Del Ben, M.; Zhao, X. S.; Mundy, C. J. Quantifying the Hydration Structure of Sodium and Potassium Ions: Taking Additional Steps on Jacob's Ladder. *Phys. Chem. Chem. Phys.* **2020**.

(44) Galib, M.; Schenter, G. K.; Mundy, C. J.; Govind, N.; Fulton, J. L. Unraveling the Spectral Signatures of Solvent Ordering in K-Edge XANES of Aqueous $Na^+$. *J. Chem. Phys.* **2018**, *149*, 124503.

(45) Baer, M. D.; Pham, V.-T.; Fulton, J. L.; Schenter, G. K.; Balasubramanian, M.; Mundy, C. J. Is Iodate a Strongly Hydrated Cation? *J. Phys. Chem. Lett.* **2011**, *2*, 2650–2654.

(46) Fulton, J. L.; Schenter, G. K.; Baer, M. D.; Mundy, C. J.; Dang, L. X.; Balasubramanian, M. Probing the Hydration Structure of Polarizable Halides: A Multiedge XAFS and Molecular Dynamics Study of the Iodide Anion. *J. Phys. Chem. B* **2010**, *114*, 12926–12937.

(47) Cauët, E.; Bogatko, S.; Weare, J. H.; Fulton, J. L.; Schenter, G. K.; Bylaska, E. J. Structure and Dynamics of the Hydration Shells of the $Zn^{2+}$ Ion from Ab Initio Molecular Dynamics and Combined Ab Initio and Classical Molecular Dynamics Simulations. *J. Chem. Phys.* **2010**, *132*, 194502.

(48) Fulton, J. L.; Kathmann, S. M.; Schenter, G. K.; Balasubramanian, M. Hydrated Structure of Ag(I) Ion from Symmetry-Dependent, K- and L-Edge XAFS Multiple Scattering and Molecular Dynamics Simulations. *J. Phys. Chem. A* **2009**, *113*, 13976–13984.

(49) Dang, L. X.; Schenter, G. K.; Glezakou, V.-A.; Fulton, J. L. Molecular Simulation Analysis and X-Ray Absorption Measurement of $Ca^{2+}$, $K^+$ and $Cl^-$ Ions in Solution. *J. Phys. Chem. B* **2006**, *110*, 23644–23654.

(50) Dang, L. X.; Schenter, G. K.; Fulton, J. L. EXAFS Spectra of the Dilute Solutions of $Ca^{2+}$ and $Sr^{2+}$ in Water and Methanol. *J. Phys. Chem. B* **2003**, *107*, 14119–14123.

(51) McCarthy, M. I.; Schenter, G. K.; Chacon-Taylor, M. R.; Rehr, J. J. Prediction of Extended X-Ray-Absorption Fine-Structure Spectra from Molecular Interaction Models:(100) Interface. *Phys. Rev. B - Condens. Matter Mater. Phys.* **1997**, *56*, 9925–9936.

(52) Chen, Y.; Fulton, J. L.; Linehan, J. C.; Autrey, T. In Situ XAFS and NMR Study of Rhodium-Catalyzed Dehydrogenation of Dimethylamine Borane. *J. Am. Chem. Soc.* **2005**, *127*, 3254–3255.

(53) Klysubun, W.; Thongkam, Y.; Pongkrapan, S.; Won-In, K.; T-Thienprasert, J.; Dararutana, P. XAS Study on Copper Red in Ancient Glass Beads from Thailand. *Anal. Bioanal. Chem.* **2011**, *399*, 3033–3040.

(54) Tyo, E. C.; Vajda, S. Catalysis by Clusters with Precise Numbers of Atoms. *Nat. Nanotechnol.* **2015**, *10*, 577–588.

(55) Yin, C.; Tyo, E.; Kuchta, K.; von Issendorff, B.; Vajda, S. Atomically Precise (Catalytic) Particles Synthesized by a Novel Cluster Deposition Instrument. *J. Chem. Phys.* **2014**, *140*, 174201.

(56) Duffe, S.; Grönhagen, N.; Patryarcha, L.; Sieben, B.; Yin, C.; von Issendorff, B.; Moseler, M.; Hövel, H. Penetration of Thin C60 Films by Metal Nanoparticles. *Nat. Nanotechnol.* **2010**, *5*, 335–339.

(57) Di Vece, M.; Palomba, S.; Palmer, R. E. Pinning of Size-Selected Gold and Nickel Nanoclusters on Graphite. *Phys. Rev. B* **2005**, *72*, 73407.

(58) Lee, S.; Lee, B.; Seifert, S.; Vajda, S.; Winans, R. E. Simultaneous Measurement of X-Ray Small Angle Scattering, Absorption and Reactivity: A Continuous Flow Catalysis Reactor. *Nucl. Instruments Methods Phys. Res. Sect. A Accel. Spectrometers, Detect. Assoc. Equip.* **2011**, *649*, 200–203.

(59) Kresse, G.; Hafner, J. Ab Initio Molecular Dynamics for Liquid Metals. *Phys. Rev. B* **1993**, *47*, 558–561.

(60) Kresse, G.; Furthmüller, J. Ab Initio Molecular-Dynamics Simulation of the Liquid-Metal-Amorphous-Semiconductor Transition in Germanium. *Phys. Rev. B* **1994**, *40*, 14251–14271.

(61) Kresse, G.; Furthmiiller, J. Efficiency of Ab-Initio Total Energy Calculations for Metals and Semiconductors Using a Plane-Wave Basis Set. *Comput. Mater. Sci.* **1996**, *6*, 15–50.

(62) Kresse, G.; Furthmüller, J. Efficient Iterative Schemes for Ab Initio Total-Energy Calculations Using a Plane-Wave Basis Set. *Phys. Rev. B* **1996**, *54*, 11169–11186.

(63) Kresse, G.; Joubert, D. From Ultrasoft Pseudopotentials to the Projector Augmented-Wave Method G. *Phys. Rev. B* **1999**, *59*, 1758–1775.

(64) Perdew, J. P.; Burke, K.; Ernzerhof, M. Generalized Gradient Approximation Made Simple. *Phys. Rev. Lett.* **1996**, *77*, 3865–3868.

(65) Zemann, J. Crystal Structures, 2nd Edition. Vol. 1 by R. W. G. Wyckoff. *Acta Crystallogr.* **1965**, *18*, 139.

(66) Zhai, H.; Alexandrova, A. N. Ensemble-Average Representation of Pt Clusters in Conditions of Catalysis Accessed through GPU Accelerated Deep Neural Network Fitting Global Optimization. *J. Chem. Theory Comput.* **2016**, *12*, 6213–6226.

(67) Jimenez-Izal, E.; Liu, J.-Y.; Alexandrova, A. N. Germanium as Key Dopant to Boost the Catalytic Performance of Small Platinum Clusters for Alkane Dehydrogenation. *J. Catal.* **2019**, *374*, 93–100.

(68) Dadras, J.; Jimenez-Izal, E.; Alexandrova, A. N. Alloying Pt Sub-Nano-Clusters with Boron: Sintering Preventative and Coke Antagonist? *ACS Catal.* **2015**, *5*, 5719–5727.

(69) Gorey, T. J.; Zandkarimi, B.; Li, G.; Baxter, E. T.; Alexandrova, A. N.; Anderson, S. L. Preparation of Size- And Composition-Controlled $Pt_nSn_x/SiO_2$ (n = 4, 7, 24) Bimetallic Model Catalysts with Atomic Layer Deposition. *J. Phys. Chem. C* **2019**, *123*, 16194–16209.

(70) Guangjing, L.; Zandkarimi, B.; Cass, A. C.; Gorey, T. J.; Allen, B. J.; Alexandrova, A. N.; Anderson, S. L. Sn-Modification of $Pt_7$/Alumina Model Catalysts : Suppression of Carbon Deposition and Enhanced Thermal Stability. *J. Chem. Phys.* **2020**, *152*, 024702–024713.

(71) Gorey, T.; Zandkarimi, B.; Li, G.; Baxter, E.; Alexandrova, Anastassia; Anderson, S. Coking-Resistant Sub-Nano Dehydrogenation Catalysts: $Pt_nSn_x/SiO_2$ (n = 4, 7). *ACS Catal.* **2020**, *accepted*, https://doi.org/10.1021/acscatal.0c00668.

(72) Sun, G.; Alexandrova, A. N.; Sautet, P. Structural rearrangements of subnanometer Cu

oxide clusters govern catalytic oxidation. *ACS Catal.* **2020**, under minor revision.

(73) Cheng, L.; Yin, C.; Mehmood, F.; Liu, B.; Greeley, J.; Lee, S.; Lee, B.; Seifert., S.; Winans, R. E.; Teschner, D.; Schlögl, R.; Vajda, S.; Curtiss, L. A. Reaction Mechanism for Direct Propylene Epoxidation by Alumina-Supported Silver Aggregates: The Role of the Particle/Support Interface. *ACS Catal.* **2014**, *4*, 32–39.

(74) Dudarev, S. L.; Botton, G. A.; Savrasov, S. Y.; Humphreys, C. J.; Sutton, A. P. Electron-Energy-Loss Spectra and the Structural Stability of Nickel Oxide: An LSDA+U Study. *Phys. Rev. B* **1998**, *57*, 1505–1509.

(75) Joly, Y. X-Ray Absorption near-Edge Structure Calculations beyond the Muffin-Tin Approximation. *Phys. Rev. B* **2001**, *63*, 125120–125129.

(76) Bunău, O.; Joly, Y. Self-Consistent Aspects of x-Ray Absorption Calculations. *J. Phys. Condens. Matter* **2009**, *21*, 345501–345511.

(77) Joly, Y.; Bunu, O.; Lorenzo, J. E.; Galéra, R. M.; Grenier, S.; Thompson, B. Self-Consistency, Spin-Orbit and Other Advances in the FDMNES Code to Simulate XANES and RXD Experiments. *J. Phys. Conf. Ser.* **2009**, *190*, 012007–012018.

(78) Ravel, B.; Newville, M. ATHENA, ARTEMIS, HEPHAESTUS: Data Analysis for X-Ray Absorption Spectroscopy Using IFEFFIT. *J. Synchrotron Radiat.* **2005**, *12*, 537–541.

(79) Halder, A.; Ha, M.-A.; Zhai, H.; Yang, B.; Pellin, M. J.; Seifert, S.; Alexandrova, A. N.; Vajda, S. Oxidative Dehydrogenation of Cyclohexane by Cu vs Pd Clusters: Selectivity Control by Specific Cluster Dynamics. *ChemCatChem* **2019**, *12,* 1307.

(80) Alyea, E. C.; Keane, M. A. The Oxidative Dehydrogenation of Cyclohexane and Cyclohexene over Unsupported and Supported Molybdena Catalysts Prepared by Metal Oxide Vapor Deposition. *J. Catal.* **1996**, *164*, 28–35.

(81) Dummer, N. F.; Bawaked, S.; Hayward, J.; Jenkins, R.; Hutchings, G. J. Oxidative Dehydrogenation of Cyclohexane and Cyclohexene over Supported Gold, Palladium and Gold–Palladium Catalysts. *Catal. Today* **2010**, *154*, 2–6.

(82) Lee, S.; Halder, A.; Ferguson, G. A.; Seifert, S.; Winans, R. E.; Teschner, D.; Schlögl, R.;

Papaefthimiou, V.; Greeley, J.; Curtiss, L. A.; Vajda, S. Subnanometer Cobalt Oxide Clusters as Selective Low Temperature Oxidative Dehydrogenation Catalysts. *Nat. Commun.* **2019**, *10*, 954.

(83) Uppireddi, K.; Westover, T. L.; Fisher, T. S.; Weiner, B. R.; Morell, G. Thermionic Emission Energy Distribution from Nanocrystalline Diamond Films for Direct Thermal-Electrical Energy Conversion Applications. *J. Appl. Phys.* **2009**, *106*, 43716.

(84) Baryshev, S. V; Antipov, S.; Jing, C.; Quintero, K. J. P.; Sumant, A. V. Ultrananocrystalline Diamond Films as a High QE Photocathode. *AIP Conf. Proc.* **2016**, *1777*, 80001.

(85) Nauert, S. L.; Schax, F.; Limberg, C.; Notestein, J. M. Cyclohexane Oxidative Dehydrogenation over Copper Oxide Catalysts. *J. Catal.* **2016**, *341*, 180–190.

(86) Hu, C.-Y.; Shih, K.; Leckie, J. O. Formation of Copper Aluminate Spinel and Cuprous Aluminate Delafossite to Thermally Stabilize Simulated Copper-Laden Sludge. *J. Hazard. Mater.* **2010**, *181*, 399–404.

(87) Ragupathi, C.; Vijaya, J. J.; Kennedy, L. J.; Bououdina, M. Nanostructured Copper Aluminate Spinels: Synthesis, Structural, Optical, Magnetic, and Catalytic Properties. *Mater. Sci. Semicond. Process.* **2014**, *24*, 146–156.

(88) Abaide, E. R.; Anchieta, C. G.; Foletto, V. S.; Reinehr, B.; Nunes, L. F.; Kuhn, R. C.; Mazutti, M. A.; Foletto, E. L. Production of Copper and Cobalt Aluminate Spinels and Their Application as Supports for Inulinase Immobilization. *Mater. Res.* **2015**, *18*, 1062–1069.

(89) Bunker, G.; Stern, E. Experimental Study of Multiple Scattering in X-Ray-Absorption Near-Edge Structure. *Phys. Rev. Lett.* **1984**, *52*, 1990–1993.

(90) Mitchell, G.; Beeman, W. W. The X-Ray K Absorption Edges of Covalently Bonded Cr, Mn, Fe, and Ni. *J. Chem. Phys.* **1952**, *20*, 1298–1301.

(91) Coster, D. Über Die Absorptionsspektren Im Röntgengebiet. *Z. Phys.* **1924**, *25*, 83.

(92) Hanson, H.; Beeman, W. W. The Mn K Absorption Edge in Manganese Metal and

Manganese Compounds. *Phys. Rev.* **1949**, *76*, 118–121.

(93) Farges, F.; Brown, G. E.; Navrotsky, A.; Gan, H.; Rehr, J. J. Coordination Chemistry of Ti(IV) in Silicate Glasses and Melts: II. Glasses at Ambient Temperature and Pressure. *Geochim. Cosmochim. Acta* **1996**, *60*, 3039–3053.

(94) Farges, F.; Brown, G. E. Ti-Edge XANES Studies of Ti Coordination and Disorder in Oxide Compounds: Comparison between Theory and Experiment. *Phys. Rev. B - Condens. Matter Mater. Phys.* **1997**, *56*, 1809–1819.

(95) Kosugi, N.; Yokoyama, T.; Kuroda, H. Polarization Dependence of XANES of Square-Planar $Ni(CN)_4^{2-}$ Ion. A Comparison with Octahedral $Fe(CN)_6^{4-}$ and $Fe(CN)_6^{3-}$ Ions. *Chem. Phys.* **1986**, *104*, 449–453.

## Table of Content

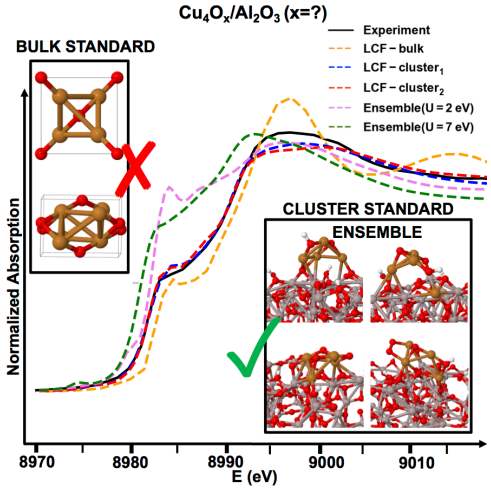


Linear combination fitting (LCF) of the experimental XANES to the global minimum structures of $Cu_4O_x/Al_2O_3$ (x = 2–5), which were obtained from DFT, is the accurate way in order to obtain the oxygen content of the cluster rather than LCF to the bulk CuO and $Cu_2O$.